Development of a reliable and low cost miniaturized Reaction Wheel System for CubeSat applications

Ricardo Gomes
ricardo.pereira.gomes@ist.utl.pt

Instituto Superior Técnico, Lisboa, Portugal
April 2016

Abstract

This paper reports the design and development of a Reaction Wheel System (RWS) with a total mass of no more than 200 grams and a minimum service life of two year. The proposed design features will enable a new classes of missions currently difficult to achieve.

The optimal design, reliability analysis, and construction of a miniaturized RWS prototype using a commercial off-the-shelf brushless DC (BLDC) motor is presented. The hardware design is described, with emphasis on the disk-rim flywheel design and on the RWS arrangement for minimum power consumption during the required orbital manoeuvres. The flywheel's mass, maximum radial and tangential stress is minimized subject to constraints on the required moment of inertia, flywheel's thickness and type of material used. The required torque and the maximum external disturbance torque acting on the satellite are estimated. A full dynamic simulation of the RWS is also presented. The controller design for the BLDC motor and the determination of the mean time to failure of the system is also one of the objectives of this paper.

This ends in a fully functional prototype, which satisfies all the constrains and requirements.

Keywords: Reaction Wheel System, Flywheel, Dynamics and Control, Development and Design, Nanosatellite, CubeSat

1. Introduction

The use of satellites for military, scientific and commercial purposes has been rising year after year.

One reason for miniaturing satellites is to reduce the cost, i.e, heavier satellites require larger rockets with greater thrust. The decreasing cost of this miniaturized satellites are making them accessible to academia and student-led projects [1]. Inside of this group of satellites there is a specific class type which has a volume of exactly one liter and a mass of no more than $1.33Kg$ - **the Cubesats** [2].

In September 2010, Geocentrix (a Canadian company) organized the first Canadian Satellite Design Challenge (CSDC) and invited twelve universities across Canada to develop a micro-satellite [3]. This challenge has contributed to an increase in expertise and training of highly-qualified personnel at several universities. To answer to this competition the University of Victoria has created the ECOSat project, which is now on the third project competition.

Magnetorquers have a full range of control at polar orbits, and become less effective at lower inclination orbits. ECOSat-III will have an orbital inclination of $i = 51.6°$. Moreover, due to the primary mission requirements a precise pointing is required, which cannot be achieved if the satellite only uses magnetorquers as a control component. Thus, the Attitude Determination and Control System (ADCS) must consist also in multiple reaction wheels that spin at a fast enough rates to allow the conservation of angular momentum to generate control torques on the rotation axis, so that the satellite can turn about this fixed axis and orient itself in the desired directions.

2. Basic concepts and equations

According to the angular kinetic equations an object that is spinning has a quantity of rotation associated with it, known as its angular momentum. The time derivative of the angular momentum of the satellite neglecting all the external perturbation torques can de written as [4],

$$I_s\dot{\omega}_B + \dot{h} = 0 \tag{1}$$

where I_s is the inertia tensor of the satellite; $\dot{\omega_b}$ is the angular acceleration vector in the satellite's fixed-body reference frame and $\dot{h} = I_{rws}\dot{\omega_{rws}}$ which is the torque generated by the RWS. This equation will allow the design and construction of a RWS able to control the attitude of the satellite.

Based on this law it will be possible to define an active system able to control the angular rate of the satellite during its orbital movement.

2.1. Desired Manoeuvre

ECOSat-III will have a circular orbit around 800 km above Earth's surface. According to ECOSat team simulations for the orbit of the satellite, using STK - AGI software, the torque needed to be provided to the satellite above Victoria around the axis of biggest inertia (Y-axis of the satellite in the fixed body reference frame), neglecting all the external perturbation torques is presented in Fig. 1.

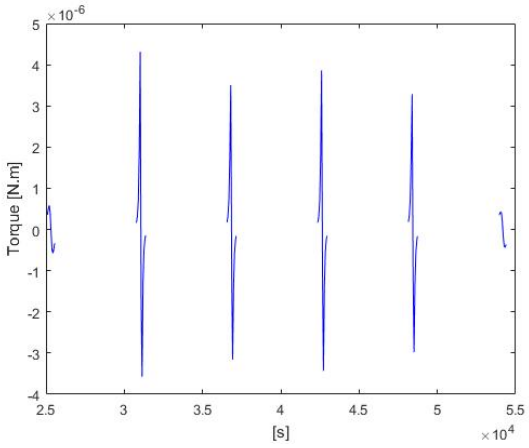

Figure 1: Torque that should be applied on ECOSat-III during its crossing above Victoria (maximum angular rate), considering the absence of external perturbation torques

However, in real space conditions, this assumption is not truly correct and several forces will exert external perturbation torques to the satellite.

3. External perturbation torques

In space there are natural forces that in turn make bodies tumble. These forces are caused by solar radiation [5], gravity gradient [6], Earth magnetic field [7] and aerodynamics [8]. In the context of attitude and control these forces are called disturbance forces [9].

Perturbation torque	Magnitude [Nm]
Gravity gradient	4.311080×10^{-8}
Aerodynamic	2.995217×10^{-7}
Solar radiation	8.261716×10^{-9}
Magnetic field	2.087731×10^{-6}
Total	2.438657×10^{-6}

Table 1: Magnitude of each principal external perturbation torque [10]

In real conditions, each kind of external perturbation torques will have a specific torque vector associated to it. It will be assumed that all the external perturbation torques are acting in the same direction simultaneously with their maximum possible magnitude, which will be replied to each axis in the body reference frame.

4. RWS Design

4.1. Motor Selection

Based on the mission objectives and on the trade-off between the several investigated motors, it was possible to conclude that FAULHABER 1202 004 BH was the best motor to be used in ECOSat's satellite [10] .

4.2. Maximum useful speed

Form the requirements and also from the simulation obtained from STK, the required torque to be provided by the RWS should be 6.64×10^{-6} N.m (see Section 2 - 3) Assuming this, a full characterization of the motor was done in order to determine the maximum useful speed at which the flywheel shall rotate [10].

In some actual space programs, specially those involving imaging satellites, the interruption of an imaging mission due to wheel zero-crossing should be avoided. Thus, it shall be found an agreement between the reliability and the agility of the RWS. Since in this case the agility does not have priority, the wheels shall be forced to operate only within the half of the speed range without sign change, i.e. $H_i = [H_{min}; H_{max}]$. This scheme is also implemented by setting the operational speed equals to half of the maximum useful speed - 18400 rpm.

4.3. Flywheel Design

The value of the maximum speed w_{max} is of primary importance in the design of the flywheel, since higher speeds result in higher centrifugal stresses which should not exceed the admissible values of the selected material for the manufacture. As modern designs require light weight, the design parameters are chosen in order to ensure minimum mass and simultaneously the minimum stresses.

4.4. Design criteria

The moment of inertia of a mass element about a given axis is proportional to the square distance between the element and its axis. In bodies of revolution larger distances imply larger circumference and areas. In sum, these factors must be investigated properly in order to achieve the optimum design for the flywheel mass considering at the same time the radial stresses at which the wheel is going to be exposed. To ensure this a rim-disk flywheel is suggested.

The major theoretical assumptions were based on the theory of the rotating disks of uniform thickness and density which were applied independently

to the disk and the rim with a suitable matching condition at the junction [11].

4.5. Simplified analytical model

As initial starting point a disk-rim flywheel were considered. It should be indicated that the flywheel is fitted with a hub around the axis of rotation for mounting around the shaft. This hub serves as a reinforcement of the disc and neglecting it in the calculation will be an approximation in the safe side.

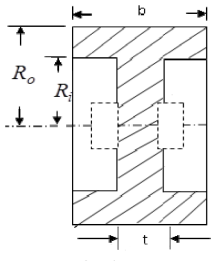

Figure 2: Disk-rim flywheel [11]

According to Bedier and Naggar [11] the tensile radial stress, σ_r, and the tensile tangential stress, σ_θ, is given by,

$$\sigma_r = \frac{A}{2} - \frac{3-\upsilon}{8}\rho\omega^2 r^2 + \frac{B}{r^2}, \tag{2}$$

$$\sigma_\theta = \frac{A}{2} - \frac{1+3\upsilon}{8}\rho\omega^2 r^2 + \frac{B}{r^2}, \tag{3}$$

where υ is the Poison's ratio of the material, ρ is the material density and A and B are arbitrary constants to be determined from the boundary conditions imposed on both the disk and the rim.

From the previous equations 2 and 3 we can easily conclude that $B = 0$, since for $B/r^2 = 0$ gives de only finite solution for the resolution of this problem.

The maximum value for the radial and the tangential stress occurs at the center of the disk, where $r = 0$. Nevertheless, there is still yet undetermined arbitrary constants $A/2$. The total centrifugal force on the rim can be given by,

$$F_c = M_{rim}\omega^2 \overline{R}_{rim} \tag{4}$$

where M_{rim} is the mass of the rim, ω is the angular velocity of the flywheel and $\overline{R}_{rim}$ is the mean radius of the rim, which can be easily computed $\overline{R}_{rim} = \frac{1}{2}(R_i + R_0)$. If the mass of the rim is assumed to be uniformly distributed, $M_{rim} = \rho\pi b(R_0^2 - R_i^2)$.

It must also be assumed the area over which this force is uniformly distributed is the contact area between the disk and the rim, given by $2\pi R_i t$. Thus, the resulting radial stress at the disk edge is given by:

$$\sigma_{r|R_i} = \frac{1}{4}\rho\omega^2 R_i^2 y(x^2-1)(x+1) \tag{5}$$

where $y = b/t$ and $x = R_0/Ri$. By using the previous Eq. 5 as a boundary condition, the solution for the value of the constant A in Eq. 2 and Eq. 3 can be easily calculated.

After determine the value of the constant A and since the maximum radial stress occurs at $r = 0$, it is easy to conclude that,

$$\sigma_{rdiskmax} = \sigma_{\theta diskmax} = \frac{A}{2} \tag{6}$$

Based on the aforementioned relations, it is now possible to define the two objective functions that shall be used in in order to determine the minimum mass, Eq. 7, and to minimize the maximum radial stress, Eq. 8 for different flywheel configurations,

$$M_{disk-rim}(R_i, y, x) = \rho\pi R_i^2 t[1 + y(x^2-1)], \tag{7}$$

$$\sigma_{r_{diskmax}}(R_i, y, x) = \rho\omega^2 R_i^2\left[\frac{3+\upsilon}{8} + \frac{1}{4}y(x^2-1)(x+1)\right]. \tag{8}$$

4.6. Shape optimization

After defining the simplified analytical model a shape optimization for the geometric parameters for the disk-rim flywheel must be considered.

The major objective to optimize is the mass of the flywheel. Another factor to be considered is the radial and tangential stress at which the flywheel will be subject which may compromise the entire RWS. Also, there are some constrains to consider.

- *Inertial constrain*: It will be assumed the non-optimized RWS configuration (worst case) in which each of the three wheels are aligned with the X,Y and Z axes w.r.t. the satellite fixed-body reference frame.

  Consequently, each wheel should be able to store angular momentum over a dynamic range of $H_{req} = 1.09 \times 10^{-3}\ Nms$. The value for H_{req} takes into consideration the integration of the maximum perturbation torque magnitude caused by any external force acting on the satellite, as well as the necessary angular momentum that should be transferred to the satellite in order to maintain the required attitude during its manoeuvre above Victoria, B.C., which takes approximately 400 seconds to complete [10]. Thus, according to Eq. 4.6, the inertia momentum of the flywheel in the direction of rotation of the wheel $I_{zz_{wheel}}$ shall be bigger than $5.533 \times 10^{-7}\ kg.m^2$.

$$I_{zz_{wheel}} \geq H_{req}\frac{30}{\pi n} - I_{zz_{motor}} \tag{9}$$

where $n = 18400\ rpm$.

- *Geometric constrain*: It was defined that the difference between the internal radius of the disk, R_i, and the external radius of the rim, R_0, should be bigger than 2 mm;

It was also concluded that aluminium has a better performance than the other materials for space application proposes not only because it is a lighter material, but also due to its mechanical properties.

The following feasible objective space graph shows several optimal solutions for the aforethought problem. Nevertheless, since the objective is to minimize the mass and simultaneously the radial stress at which the structure will be subject the optimum selected solution corresponds to we one given, see Fig. 3.

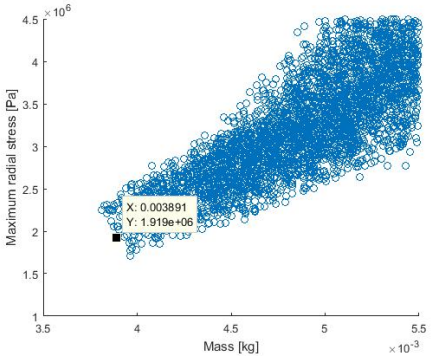

Figure 3: Feasible objective space graph for aluminium

In the real flywheel a hub around the axis of rotation for mounting the shaft and to serve as a reinforcement of the disc is necessary. The thickness of the disk is 1 mm, which will be the value used for the thickness of the hub. Moreover, the real flywheel will also display a small difference when compared to the theoretical disk-rim flywheel that was designed. This difference relates to the use of fillets. It was defined that its fillet shall have a radius of 0.5 mm. This value was set in order to facilitate the manufacture of the flywheel.

4.7. Pyramid configuration

If 3-axis stabilization is required, three reaction wheels with mutually perpendicular axes would be used. For redundancy reasons a fourth wheel is normally added to maintain full 3-axis controllability when one wheel fails [12].

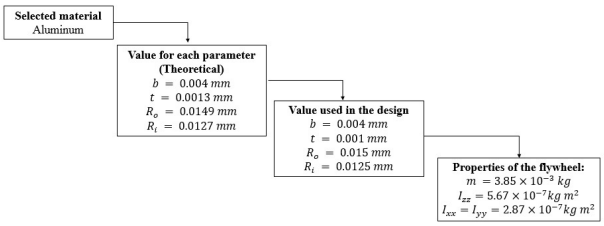

Figure 4: Optimal solution design for the flywheel using aluminium

Pyramidal configuration is an approach that can be considered as a specific arrangement of actuators in satellites and attitude simulators [13] [14].

Nevertheless, there are several factor in the RWS configuration that should be consider to optimize the all system. The major design criteria is to minimize the power consumption of the system during the attitude manoeuvre [13]. Obviously, choosing a proper skew angle will lead to achieve minimum power consumption. Also, other criteria such as maximum rotational speed of the wheels can be assumed as the main goal in this optimization as well the rotation necessary, without going into saturation, to maintain the angular momentum if one of the four wheels fail. Only the first criteria described will be consider, i.e. the minimization of the power consumption. The scheme of a pyramid configuration is depicted in Fig. 5.

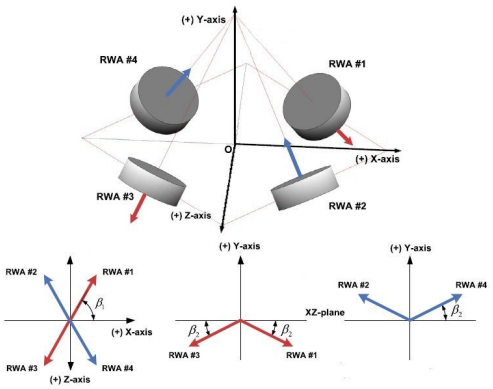

Figure 5: Pyramid configuration [15]

Assuming the configuration aforementioned, it is possible to arrange the applied wheel angular momenta of the individual wheels in a column vector $H_w = [H_1 H_2 H_3 H_4]^T \in \Re^4$, where the subscript W denotes the n-dimensional wheel frame. The transformation from the wheel frame to the body frame is given by the $3 \times n$ distribution matrix W, whose columns are unit vectors in the body frame w_i, along the spin axes of the wheels [16]:

$$W = [\widehat{w_1}, ..., \widehat{w_4}]_{3\times 4}. \tag{10}$$

Thus, the total angular momentum generated by the RWS is $H_t \in \Re^3$ and are related with the angular momentum of each individual wheel according to

$$H_t = WH_w, \tag{11}$$

and the torque relationship can be written as

$$T_t = WT_w, \tag{12}$$

where $T_t \in \Re^3$ is the total torque and $T_w = [T_1 ... T_4]^T \in \Re^4$ is the torque vector of the wheel array. Thus, assuming the specific configuration shown in Fig. 5, the distribution matrix W can be expressed as,

$$W = \begin{bmatrix} \cos\beta_1 \cos\beta_2 & -\cos\beta_1 \cos\beta_2 & -\cos\beta_1 \cos\beta_2 & \cos\beta_1 \cos\beta_2 \\ -\sin\beta_2 & \sin\beta_2 & -\sin\beta_2 & \sin\beta_2 \\ -\sin\beta_1 \cos\beta_2 & -\sin\beta_1 \cos\beta_2 & \sin\beta_1 \cos\beta_2 & \sin\beta_1 \cos\beta_2 \end{bmatrix} \tag{13}$$

The momentum of each wheel H_i, where $i = 1, ..., 4$ is assumed to be limited as $H_i \in [H_{min}, H_{max}]$, and the wheel torque T_i, with $i = 1, ..., 4$ as $T_i \in [T_{min}, T_{max}]$.

Based on the transformation matrix, W, presented in Eq. 13 it is possible to determine the velocity each wheel shall rotate in order to maintain the required angular momentum of the satellite during a specific manoeuvre.

It will be assumed all the angular momentum generated by the RWS is transmitted to the satellite. As it was already specified the major variation on the angular momentum will occur above the Island of Vancouver.

4.8. Power analysis

After defining the pyramid configuration as the one that is going to be used, the goal is now find the optimal angle β_1 and β_2 that minimizes the power consumption of the system. This configuration will be optimized for the manoeuvre above the Vancouver Island. In this the y axis of the RWS should be aligned with the y axis of the satellite w.r.t. the body fixed reference frame, since this is the axis, over which, the system should shall the biggest manoeuvrability. The determination of the power consumption was done by using the variation of the total angular momentum. Based on that, it was possible to determine the final angular velocity of each wheel assuming the simplified DC model already described, which are related with the necessary voltage to be provided to each motor. Several simulations to different

β_1 and β_2 angles were performed in order to determine the configuration that generates the lowest power consumption (see Fig. 6).

It was possible to conclude that the best configuration which minimizes the power consumption for the required manoeuvre implies that $\beta_1 = 45°$ and $\beta_2 = 60°$.

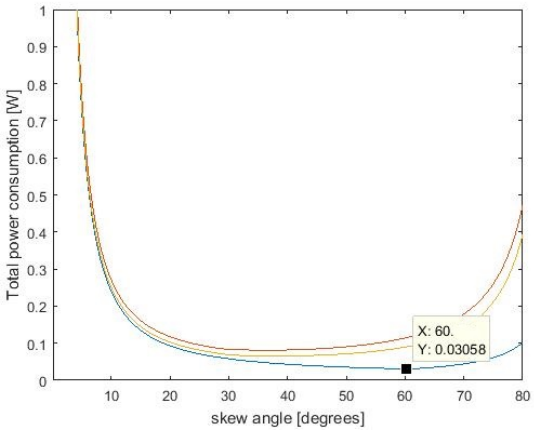

Figure 6: RWS power neglecting the electronics power consumption as function of the skew angle. ($\beta_1 = 45\ deg$ in blue; $\beta_1 = 40\ deg$ in green; $\beta_1 = 30\ deg$ in red). Minimum power consumption for $\beta_1 = 45\ deg$ and $\beta_2 = 60\ deg$

5. Internal Disturbances

There are two main disturbances that may affect the dynamics of the RWS. Both of them should be analysed in order to determine if they can disturb the entire system. The main sources of this internal disturbances are [17],

- **Axial play in the shaft of the motor**. From the specifications of the selected COTS motor - FAULHABER 1202 004BH, the axial radial play in the motor axle, δ_{play}, will have a value of 0.011 mm at the bearing exit. Again according with the specification the distance between the origin of the motor and the bearing exit, $d_{bearing}$ has a length of 0.074 mm. Thus, according to this data the maximum deflection of the motor's shaft is given by,

$$\theta_{axle} = \tan\left(\frac{\delta_{play}}{d_{bearing}}\right) \tag{14}$$

- **Flywheel manufacturing tolerances**. It will be assumed that the center of mass of the real flywheel will have a shift in relation to the perfect model. This shift for simplicity is going to be caused due to tolerance manufacturing errors. These manufacturing errors will be represented by an angle which correlates the tolerance in the width of the rim with the deflection of the center of mass. This angle is obtained assuming a variation in the flat feature of $\delta_{tolerance} = 0.01$ mm

$$\theta_{man} = \tan\left(\frac{\delta_{tolerance}}{r_{wheel}}\right) \tag{15}$$

The following Fig.7, shows how the sources of this internal disturbances will deflect the flywheel relatively to a perfect RWS model.

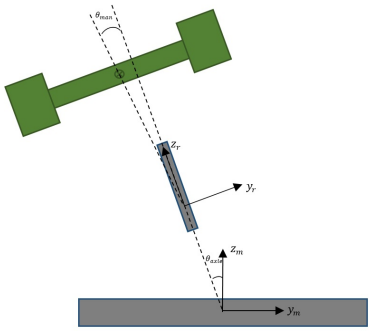

Figure 7: Deflection angles representation due to internal disturbance torques sources in the Reaction Wheel

Thus, it is necessary to assess the effect these error angles may have in the RWS. The major objective to compute is the resulting worst-case accelerations of the flywheel with respect to the origin of the body-fixed motor reference frame.

5.1. Mathematical representation

The objective here is to assess the acceleration of the flywheel center of gravity in the body-fixed reference frame. Thus, the position vector of the flywheel center of gravity, r_w^M, expressed in the body-fixed motor reference frame is given by,

$$r_w^M = r_o^M + R^{M/R} r_w^r \tag{16}$$

Where r_o^M is the position vector from the body-fixed motor reference frame origin to the origin of the rotor reference frame. The motor reference frame origin is considered to be in the geometric center of the motor's cage, ı.e 0.74 mm above its base and the origin of the rotor reference frame is considered to be 1 mm above the base of the motor shaft. Assuming this, $r_o^M = [0; -z_o sin(\theta_{axle}); z_o cos(\theta_{axle})]$, where $z_o = 1.74$ mm is the distance to the flywheels base relative to the origin of the motor reference frame. The variable r_w^r is the position vector from the origin of the rotor reference frame to the flywheel center of mass expressed in the rotor reference frame. This vector is written as, $r_w^r = [0; -z_w sin(\theta_{man}); z_w cos(\theta_{man})]$, where $z_w = 2.477$ mm is the distance from the origin the rotor reference frame (flywheel's base) to the flywheels center of mass. This value was obtained using ANSYS Workbench. The rotation matrix $R^{M/R}$ transforms a vector expressed in the rotor reference frame in the motor reference frame.

$$R^{M/R} = \begin{bmatrix} 1 & 0 & 0 \\ 0 & \cos\theta_{axle} & -\sin\theta_{axle} \\ 0 & \sin\theta_{axle} & \cos\theta_{axle} \end{bmatrix} \tag{17}$$

Nevertheless, it shall be consider that the motor is rotating around its Z-axis with speed ω, which will affect the temporal evolution of the acceleration vector in the motor reference frame. Thus, a time-dependent transformation matrix $R^{\omega t}$ shall be added to Eq. 16.

$$R^{\omega t} = \begin{bmatrix} \cos\omega t & \sin\omega t & 0 \\ -\sin\omega t & \cos\omega t & 0 \\ 0 & 0 & 1 \end{bmatrix} \tag{18}$$

This means Eq. 16 shall be re-written as

$$r_w^M = r_o^M + R^{M/R} R^{\omega t} r_w^r \tag{19}$$

The instantaneous velocity of the flywheel center of gravity with respect to the motor origin is obtained by taking the derivative of Eq. 19:

$$v_w^M = \frac{dr_w^M}{dt} = \dot{r}_o^M + \Omega \times r_o^M + R^{M/R} R^w \dot{r}_w^r + \Omega \times (R^{M/R} R^w r_w^r) \tag{20}$$

Thus assuming that $\dot{r}_o^M$ and $\dot{r}_w^r$ are fixed in time within their respective reference frames, Eq. 20 can be simplified to:

$$v_w^M = \Omega \times r_o^M + \Omega \times (R^{M/R} R^w r_w^r) = \Omega \times r_w^M \tag{21}$$

The instantaneous acceleration of the center of gravity in the body-fixed motor reference frame can then be expressed by taking the first derivative of Eq.21

$$a_w^M = \frac{dv_w^M}{dt} = \dot{\Omega} \times r_w^M + \Omega \times \dot{r}_w^M + \Omega \times \Omega \times r_w^M \tag{22}$$

Since $\dot{r}_w^M$ is fixed in time, Eq. 23 will be simplified as,

$$a_w^M = \frac{dv_w^M}{dt} = \dot{\Omega} \times r_w^M + \Omega \times \Omega \times r_w^M \tag{23}$$

where,

$$\dot{\Omega} = \begin{bmatrix} 0 \\ -\dot{\omega}\sin\theta_{axle} \\ \dot{\omega}\cos\theta_{axle} \end{bmatrix} \tag{24}$$

$$\Omega = \begin{bmatrix} 0 \\ -\omega\sin\theta_{axle} \\ \omega\cos\theta_{axle} \end{bmatrix} \tag{25}$$

Again, assuming that the origin of the motor reference frame is the pivot point of the motor axle, the angular acceleration can be easily defined by

$$\alpha_w^M = r_w^M a_w^M \tag{26}$$

5.2. Disturbance torques

With the disturbance force applied on the flywheel center of gravity, the disturbance torque, T^{fw}, acting on the motor reference frame origin can be calculated,

$$T^{fw} = I_w^M \alpha_w^M \tag{27}$$

where I_w^M represents the inertia tensor of the flywheel w.r.t. the body-fixed motor reference frame. However, there is only data available for the moment of inertia tensor of the flywheel w.r.t the body-fixed flywheel reference frame. Thus, a transformation of the inertia tensor shall be considered. For simplicity the moment of inertia of the motor will be neglected. This implies that,

$$I_w^M = R^{M/R} R^{wt} (R^{R/fw} I_{fw} (R^{R/fw})^t + I_{r_w^r}) (R^{M/R} R^{wt})^t + I_{r_o^M} \tag{28}$$

where I_{fw} is the diagonal inertia matrix of the flywheel; $R^{R/fw}$ is the transformation matrix that transforms the inertia tensor expressed in the flywheel's reference frame in the rotor reference frame; $I_{r_w^r}$ is the additional moment of inertia due to the translation of the reference frame from the flywheels center of mass to the rotor reference frame and similarly $I_{r_o^M}$ is the additional moment of inertia due to the translation of the reference frame from the rotor reference frame to the motor reference frame. The index ^{t} denotes the transpose matrix.

To assess the impact of the disturbance torque on the satellite the maximum angular displacement relatively to its desired pointing position, caused by this internal disturbances, shall be determined.

Thus, the angular displacement around the $y+$ axis w.r.t the satellite's body-fixed reference frame shall be determined, since any angular displacement around this axis will have a bigger impact on the satellite pointing precision than the angular displacement generated around the other axes. First the total disturbance torque is converted into corresponding angular acceleration vector of the satellite, assuming all the torque generated by the RWS was transferred to the satellite. The double integration over time of this parameter will assent to determine the maximum angular displacement, δ_{sat}, relatively to the pointing position the satellite will suffer when the active control system, the RWS, is activated and the wheels rotate at a certain speed.

$$\delta_{sat} = \int \int \left(I_b\right)^{-1} T^{fw} dt \tag{29}$$

To verify this disturbances it is going to be assumed that all the reaction wheels are rotating at a random speed, between 5000 and 20000 rpm. Assuming the previous described operating mode, and a random value for the phase perturbation component of each wheel, it is possible to draw a scheme of the angular displacement of the satellite around the y-axis w.r.t the satellite body-fixed reference frame (see Fig. 8).

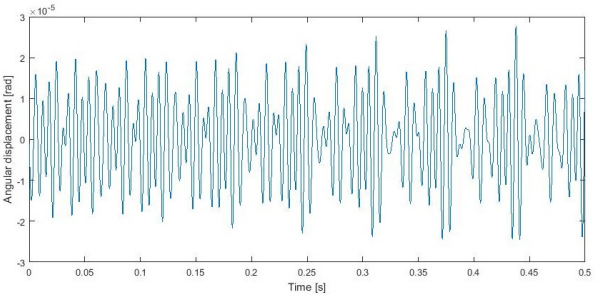

Figure 8: Angular displacement of the satellite around the y-axis w.r.t. the satellite body-fixed reference frame

5.3. Analysis of the modulated results

At 18400 rpm the calculated amplitude of the resulting disturbance torques is in the order of magnitude of 10^{-3} Nm, whereas the maximum external disturbance torques are in the order of magnitude of 10^{-6} Nm.

Then, a first analysis may lead to conclude that the internal disturbances caused by the RWS will make its use impossible. Nevertheless, since the disturbances originated by the RWS are periodic, the absolute impact on the satellite attitude will be negligible. This is confirmed by Fig. 8, which shows that, at a random velocity of rotation for each wheel, the impact of the angular displacement of the satellite relatively to the desired point can be negligible. Moreover, the pointing precision required for ECOSat's mission is approximately 2°, which is bigger than the maximum oscillation induced in the satellite by this disturbing internal forces - about 10^{-3} degrees, meaning there is no need to increase the controllability of this system. This confirms that the effect of this disturbing forces can be considered negligible.

6. Control of the RWS

BLDC motors have been used in different applications such as industrial automation, automotive, aerospace, instrumentation and appliances since 1970's [18]. BLDC motor is a type of DC motor which commutation is done electronically instead of using brushes [19]. In this section the overall system model are going to be explored as well as its response to a desired input. Subsequently a close-loop PID controler will be designed. A BLDC motor can be modulated in a similar manner as a

three-phase synchronous machine, but since there is a permanent magnet mounted on the rotor, some of their dynamic characteristics are different [19]. A modelling based on an abc phase variable is more convenient for this motors than using d-q axis [18]. Nevertheless, some assumptions should be made to the model in order to simplify it:

- Magnetic circuit saturation is ignored;
- Stator resistance, self and mutual inductance of all phases are equal and constant;
- Hysteresis and eddy current losses are eliminated;
- All semiconductor switches are ideal;

Then, the voltage equation of a BLDC motor can be expressed as:

$$V_a = Ri_a + L\frac{di_a}{dt} + E_a, \tag{30a}$$
$$V_b = Ri_b + L\frac{di_b}{dt} + E_b, \tag{30b}$$
$$V_c = Ri_c + L\frac{di_c}{dt} + E_c, \tag{30c}$$

where, L is the armature self inductance [H]; R is the armature terminal resistance [Ω]; V_a, V_b, V_c are the terminal hase voltage [V]; i_a, i_b and i_c are the motor input current [A] and E_a, E_b and E_c are the back-EMF voltage of the motor for each phase.

In a three-phase BLDC motor, the back-EMF is function of the rotor position and the back-EMF voltage of each phase has 120 deg phase different angle difference so equation of each phase should be,

$$e_a = K_w f(\theta_e)\omega, \tag{31a}$$
$$e_b = K_w f(\theta_e - 2\pi/3)\omega, \tag{31b}$$
$$e_c = K_w f(\theta_e + 2\pi/3)\omega, \tag{31c}$$

where K_w is the back EMF constant of one phase $[V/rad.s^{-1}]$

The electrical and mechanical torque can be related by,

$$\theta_e = \frac{p}{2}\theta_m \tag{32}$$

Moreover the $F(\theta_e)$, which is the back-EMF reference function which has trapezoidal shape and maximum magnitude of ±1 can be represented by,

$$f(\theta_e) = \begin{cases} 1, & \text{if } 0 \le \theta_e < 2\pi/3 \\ 1 - \frac{6}{\pi}(\theta_e - 2\pi/3), & \text{if } 2\pi/3 \le \theta_e < \pi \\ -1, & \text{if } \pi \le \theta_e < 5\pi/3 \\ -1 + \frac{6}{\pi}(\theta_e + 5\pi/3), & \text{if } 5\pi/3 \le \theta_e < 2\pi \end{cases} \tag{33}$$

The total electromagnetic torque output can be represented as the summation that of each phase,

$$T_e = T_a + T_b + T_c \tag{34}$$

where,

$$T_a = K_t i_a f(\theta_e), \tag{35a}$$
$$T_b = K_t i_b f(\theta_e - 2\pi/3), \tag{35b}$$
$$T_c = K_t i_c f(\theta_e + 2\pi/3), \tag{35c}$$

The mechanical dynamic equation of the motor can be now correlated with the electromagnetic torque,

Thus, the mechanical torque provided by the wheel can be expressed by the following equation,

$$Te - T_i = J\frac{d\omega_m}{dt} + \beta\omega_m \tag{36}$$

Based on the assumptions previously described it is now possible to create a valid model of the overall system. This actuator will have an input a $[3 \times 1]$ vector, which corresponds to the required torque that shall be applied to each axis in the satellite's body-fixed reference frame, T_{in}. The variable T_{out} is a $[3 \times 1]$ vector which corresponds to the real torque delivered by the actuator to the satellite.

A schematic representation of the RWS model can be seen in Fig. 9. Inside each RW block there is the overall model of the each motor and respective flywheel. Both matlab functions are responsible to convert torque vector, T_{in}, in the torque each wheel should delivered.

The transformation from the wheel body frame is given by the $3 \times n$ distribution matrix W, already mentioned. This means that in MATLAB Function1 a pseudo-inverse of the mentioned matrix shall be used, in order to determine the torque vector of the wheel array.

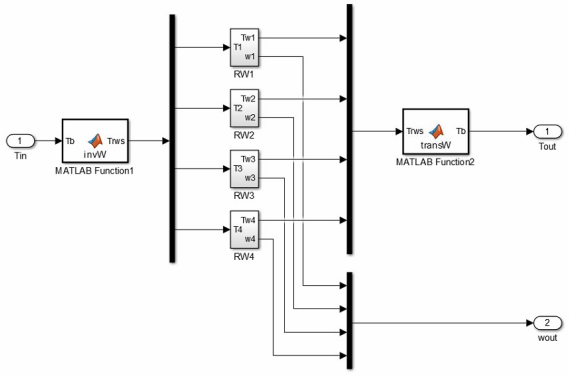

Figure 9: Overall RWS simulink block

Accordingly to the satellite requirements and the calculations already performed the minimum torque that shall be delivered around the y-axis of the satellite w.r.t. the body reference frame above Victoria shall be $T_y = 6.8 \times 10^{-6}$ Nm. It is difficult to estimate which torque is necessary to apply to the X and Y-axis, since only the upper bound of the perturbation torques caused by external factors were defined. Thus, it is going to be conjectured that the necessary torque needed will have a magnitude similar to the upper bound torques defined by the external perturbation forces. In sum, it will be assumed for the simulation a constant value of $T_x = T_z = 2.33 \times 10^{-6}$ Nm w.r.tm the satellite's fixed-body reference frame will be considered.

In this simulation to have more realistic results the update rate of the actuator variables will have a step size of 0.1 s, which will be the update rate of the real system to be implemented in ECOSat-III.

The RWS is projected based on the maximum torque that should be provided by the system. Each main manoeuvre above Victoria, B.C, takes approximately 400 s to complete. This means that the RWS should be operational and outside the saturation limits in order to guaranty the maximum pointing precision, for at least during this time. It is advisable to proceed to the desaturation of the wheel before this manoeuvre, as well as to start the manoeuvre above Victoria with the wheels rotating at its nominal speed, in order to increase the speed range available and prevent saturation.

In normal conditions, ı.e if all the wheels are operational, for the manoeuvre already specified the RWS will entered into saturation only after 600 s, as it can be seen in Fig. 10.

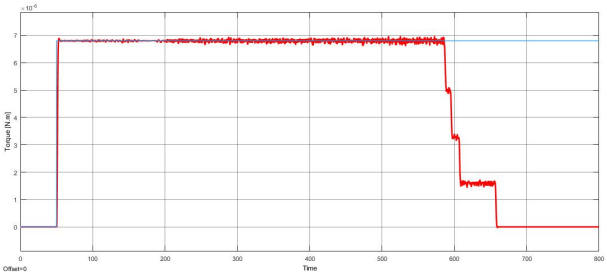

Figure 10: Torque generated in the Y-axis direction by the overall RWS w.r.t. the satellite's body-fixed reference frame in normal conditions until saturation

Considering the failure of the wheel number #1, the following figure is obtained,

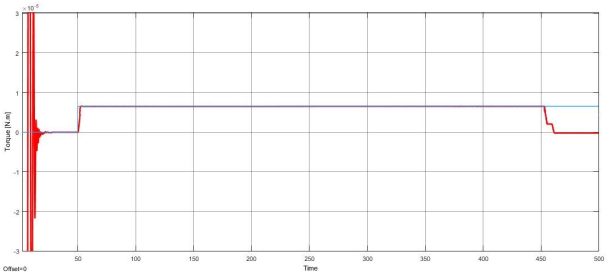

Figure 11: Torque generated in the Y-axis direction by the overall RWS w.r.t the satellite's body-fixed reference frame assuming wheel #1 has failed until saturation

The initial oscillating torque presented in the beginning of the simulation is related to the fact that the wheel failure was considered exactly after the switch on of the system. This torques in this case can not be cancelled, since it is impossible to generate a null space total torque vector.

Exactly as in the normal conditions, one shall assume that a constant torque will be required during the orbital manoeuvre above Victoria. That step was defined at $t = 50\ s$. As observed in Fig. 11, the system will take approximately 400 s to reach saturation, which is in the boundary of the defined limit. Nevertheless, this will not derail the RWS project, since this graphs were generated assuming worst case conditions. This means that the pointing precision shall not be affected, neither if one of the wheels fail.

7. Mean Time to Failure

Bearing life is an important factor to determine the survivability of the satellite under normal conditions. The modified L'_{10} formula gives the estimated mean time to failure of the bearings under normal conditions,

$$L'_{10} = a_1 a_2 \left(\frac{C_r}{P_r}\right) \times \frac{10^6}{n \times 60 \times 24 \times 365} \tag{37}$$

where, a_1 is the adjustment factors for reliability: a_2 is the adjustment factor for operating conditions; C_r is the basic dynamic radial load [N] and P_r is the dynamic equivalent radial load [N] and n corresponds to the rotational speed of the rotor [rpm]. After some simple computations for a reliability of 99% it was concluded that for the current system $L'_{10} = 2.3 years$. The value for the basic rating life previously determined ensures that the satellite shall have success in its 2 years mission. Moreover, the use of four motors in a pyramidal configuration instead of three motors oriented according each axis in the body reference frame guaranties a redundant system, and consequently ensures qualitatively the increase of the life span of the RWS.

8. Conclusions

First, an analysis of the requirements were made in order to determine the main characteristics of the RWS. Next, the calculation of the perturbation torques enabled to determine the maximum torque expected to be delivered by the RWS during its orbital movement.

Succeeding the motor selection, an optimization of the disk-rim flywheel design was performed based on the minimization of its mass and radial stress. The process here developed for the design of the flywheel can be applied to other industrial sectors. The optimal RWS configuration in order to minimize the power consumption was also obtained. This analysis let to the conclusion that a pyramid configuration would be the best trade-off between the system's redundancy and its power consumption.

The analysis based on the simulink model confirmed the viability of the system. It has been shown that a good and fast response response for the desired input torques to be provided by each wheel is achievable. Moreover, the mean time until the system reaches the saturation is under the design limits.

Finally, a MTTF analysis was performed in order to determine with a reliability of 99% if the future RWS would survive for at least during two years in space under nominal conditions.

In conclusion, it has been demonstrated that is possible to construct and developed a low-cost and reliable RWS to be implemented on a CubeSat.

9. Future Work

The following research aspects should be considered and implemented in order to achieve the final RWS assembly:

a) Experimentally verify all the predictions in order to evaluate and validate the data obtained.

b) Promote a joint collaboration between the faculty of Victoria and FAULHABER company.

c) It would be very usefull to develop an health monituring system for each reaction wheel.

d) Evaluate and perform all the tests needed in order to space qualify this technology.

References

[1] E. Buchen and D. DePasquale, "2014 Nano and Microsatellite Market Assessment," SpaceWorks Enterprises, Inc., 2014.

[2] M. Swartwout, "Cubesat Design Specification R.12," in *The Cubesat Program*, California Polytechnic State University, 2009.

[3] J. Lousada, "Design and development of the ECOSat's Attitude Determination and Control System (ADCS) onboard software," Master's thesis, Instituto Superior Técnico, Lisboa, 2013.

[4] S. Nodehin and U. Farooq, "Satellite atitude control using three reaction wheels," *American Control Conference, Seattle*, 2008.

[5] R. Bohling, J. Carrol, J. Clark, D. DeBra, *et al.*, *Spacecraft Radiation Torques*. NASA, Space Vehicle Design Criteria, May, 1969.

[6] A. Sabroff, J. Carrol, J. Clark, D. DeBra, *et al.*, *"Spacecraft Gravitational Torques"*. NASA, Space Vehicle Design Criteria, May, 1969.

[7] J. Nocedal and S. J. Wright, *"Numerical optimization"*. Springer, 2^{nd} ed., 2006. ISBN:978-0387303031.

[8] J. Clark, D. DeBra, R. Bohling, J. Carrol, *et al.*, *"Spacecraft Atmospheric Torques"*. NASA, Space Vehicle Design Criteria, May, 1969.

[9] J. Wertz, *"Spacecraft Attitude Determination and Control"*. Reidel, 1978.

[10] R. Gomes, "Development of a reliable and low-cost Reaction Wheel System for CubeSat applications," Master's thesis, Instituto Superior Técnico, Lisboa, 2016.

[11] I. K. B. Bedier, El Naggar, "Disk-rim flywheel of minimum weight," 2011. Journal of american science edition 7.

[12] H. Steyn, *"A multi.mode attitude determination and control system for small satellites"*. PhD thesis, Stellenbosch University, 1995. PhD Thesis.

[13] H. Yoon, H. H. Seo, and H.-T. Choi, "Optimal uses of reaction wheels in pyramid configuration using new minimum finity-norm solution," *Aerospace Science and Technology, ELSEVIER*, 2014.

[14] P. Goel, "Auto Reconfiguration of Reaction Wheels in IRS," *IEEE Transactions on Aerospace and Electronic Systems*, no. 1, pp. 160–163, 1985.

[15] A. Shirazi and M. Mirshams, "Pyramidal reaction wheel arrangement optimization of satellite attitude control subsystem for minimizing the power consuption," *International Journal of Aeronautical and Space Sciences*, 2014.

[16] F. Markley and J. Crassidis, *"Fundaments of Spacecraft Attitude Determination and Control"*. Springer, Space Technology Labrary, 2014.

[17] A. G. Hoevenaars, "Design, Integration and Verification of the Delfi-n3Xt Reaction Wheel System," Master's thesis, Delft University of Technology, Delft, 2012.

[18] A. Tashakori and N. Hosseinzadeh, "Modeling of BLDC Motor with Ideal Back-EMF for Automotice Applications," *Proceeding of the World Congress on Engineering, Vol II*, 2011.

[19] G. Prasad, N. Ramya, P. Prasad, and G. Tulasi, "Modelling and Simulation Analysis of the Brushless DC Motor by using MATLAB," *International Journal of Innovative Technology and Exploring Engineering (IJITEE), Vol.1, Issue-5*.